DOI 10.1007/s11595-016-1540-3

Effects of Heating and Hot Extrusion Process on Microstructure and Properties of Inconel 625 Alloy

LIU Dexue[1,2], CHENG Xiaowei[1,2], ZHANG Xiao[1,2], DING Yutian[1,2]

(1.School of Material Science and Engineering, Lanzhou University of Technology, Lanzhou 730050, China; 2. State Key Laboratory of Advanced Processing and Recyling of Nonferrous Metals, Lanzhou 730050, China)

Abstract: The effects of the heating process and hot extrusion on the microstructure and properties of inconel 625 alloy were studied. The experimental results showed that the properties of Inconel 625 alloy could be improved through the heating process and hot extrusion concomitant with a reduced corrosion rate. The $M_{23}C_6$ carbide, generated in the heating process, was retained and distributed at the grain boundary during the process of hot extrusion, which had an important influence on both elongation and corrosion resistance. The improvement of the comprehensive properties of the material, as measured by a tensile test at room temperature, was correlated with the dissolution of segregation Nb. A typical ductile fracture changed to a cleavage fracture where secondary cracks could be clearly seen. With the increase of the extrusion ratio, the real extrusion temperature was higher, which led to more dissolution of the $M_{23}C_6$ carbide, decreased the number of secondary cracks, enhanced the effect of solid solution strengthening, and reduced the intergranular corrosion rate. Under the condition of a high extrusion ratio and a high extrusion speed, the less extrusion time made it possible to obtain organization with a smaller average grain size. Moreover, in this case, the $M_{23}C_6$ carbide and segregated Nb did not have enough time to diffuse. Thus all samples exhibited medium strengths and corrosion rates after extrusion.

Key words: Inconel 625 alloy; hot extrusion; mechanical property; microstructure evolution

1 Introduction

Inconel625 alloy, a Nb and Mo-Modified Ni-Cr-Fe based superalloy, has been widely used in gas tubine[1] and jet engines with service temperatures up to 923K because of its high temperature strength and corrosion resistance[2,3]. At present, some researches are focusing on the microstructure evolution and high temperature properties of Inconel 625 alloy, and plastic deformation of nickel-base superalloy is paid more attention to develop its comprehensive performance.

As is known to all, there are many advantages to produce tubes by the method of hot extrusion, for example the small machining allowance, low surface roughness, and high dimensional accuracy. It has been concluded that the tensile strength of extruded billet has been increased and also homogeneous distribution of reinforcement has been improved than casting blank [4,5]. It is mature that extrusion technology was applied in aluminum, copper and some other alloys[6], and complex shape parts could be deformed by automatically controlling technique using a computer. However, the interface between the mold and nickel-based alloy is very special during hot extrusion, which leads to sticking each other and produces the phenomenon such as surface scratches, tear and stuffy car[7]. In addition, because there are many types of strengthening phases in nickel base alloy[8,9], the crystal structure of strengthening phase is also different. Thus, the precipitation temperatures of different precipitates are limited in a small range. What more important is that the phase transformation could be easily irritated when the material was processed at high temperature[10]. All of that make the deformation conditions and parameters difficult to control for the nickel-base superalloy and it could be classified as so-called difficult deformation alloy even though it has excellent ductility. The mechanism of a relatively higher deformation temperature and the special microstructure evolution in a narrow

(Received: Nov. 12, 2015; Accepted: Jan. 5, 2016)

LIU Dexue (刘德学) : Assoc. Prof.; Ph D; E-mail: dexeliu@hotmail.com

Funded by the National Natural Science Foundation of China (Nos.51664041 and 51365029), the Gansu Science and Technology Support Program-industrial Category (No.1604GKCA038), the Fundamental Research Funds for the Universities in Gansu Province, and the Program for Major Projects of Science and Technology in Gansu Province (No. 145RTSA004)

heating temperature range need to be revealed. Above mentioned characteristics of nickel-base alloy make themselves sensitive to the deformation speed and deformation temperature. At present, a lot of work has been done to investigate the deforming mechanism of nickel-based alloy. The processing properties of a variety of nickel base alloys, which include IN690, IN718, and IN625, and so on[11-14], are studied to obtain the hot forming properties by hot compassing test. As for Inconel 625 alloy, primary nucleation mechanism with bulging of the original grain boundaries becomes the operating mechanism of dynamic recrystallization (DRX) in the process of hot deformation[15], whilst adiabatic shear band emerges with a low temperature and high strain rate, which affects markedly the mechanical properties of the materials[16]. High strain rate is conducive to refine the organization, which has been widely accepted as an important conclusion so far. Moreover, some researchers have conducted experiments to extrude a tube of Inconel 625 alloy and analyzed the microstructural evolution based on the extrusion parameters[13]. However, the extrusion ratio and the size of the extrusion are smaller than those of the other metals previously extruded, and relatively less work has been carried out on the microstructure and properties affected by both the heating process and hot extrusion.

In the present study, large diameter tubes and bars of Inconel 625 alloy were obtained by hot extrusion at 1 160-1 180 ℃. In order to guarantee extrusion smooth, glass lubricant was used to lubricate. The two types of speed, 45 mm/s and 100 mm/s, were selected. Extrusion ratio was 3.61-9.26. The effect of hot extrusion parameters on the formability was researched, the evolution of microstructure and the improvement of properties during the whole extrusion process were analyzed emphatically. This work aims to demonstrate the influence of the heating process and parameters of extrusion on microstructure and properties of Inconel 625 alloy, which is conducive to the actual production.

2 Experimental

2.1 Preparation of materials

Inconel 625 billet for hot extrusion was electroslag remelting (ESR) ingot with preform forging. The chemical composition of the billet is listed in Table 1, the microstructure is shown in Fig.3(a).

2.2 Hot extrusion

The billet of Inconel 625 alloy was cut into cylinders with a diameter of 247 mm for hot extrusion in the nominal pressure of 31.5 MN horizontal extrusion presses. A combination of the parameters of the extrusion machine and hot workability of the Inconel 625 alloy was used to guide the hot extrusion [16], preheat temperature was controlled between 1 160-1 180 ℃ and a three-stage preheating was used before hot extrusion. Firstly, the billet was heated to 850-880 ℃ in the annular furnace heating for about 4 hours. This temperature range was under dynamic recrystallization temperature, and only reversion occurred to reduce the residual stress of the billet, and the phase transformation was limited; Secondly, the preheated billet was delivered to a induction furnace and heated to about 1 080 ℃ for 5 min. The purpose of this heating was mainly for expansion, ensuring that the extrusion punch needle can get into the blank hole, minimizing the common errors. The last heating procedure is called the induction reheating, the final billet would be heated to 1 160-1 180 ℃ for 5 min. The detailed extrusion parameters are listed in Table 2. The 1# and 3# rod samples had a same extrusion speed of 45 mm/s and different extrusion ratio of 3.61 and 5.04, respectively. The extrusion ratio of 2# tube samples was 6.06, and its extrusion speed was 100mm/s. After completion of hot extrusion, the extrusions were cooled by air cooling to room temperature. Three samples, 1#, 2#, and 3#, were extruded successfully and smoothly,

Table 1 Chemical composition of Inconel 625 superalloy/wt%

C	Cr	Ni	Co	Mo	Al	Ti	Fe	Nb	Si	Mn	S	P	Cu
0.042	21.77	60.63	0.19	8.79	0.21	0.40	3.68	3.75	0.12	0.20	0.0006	0.006	0.06

Table 2 Hot extrusion process parameter of Inconel625 superalloy

No.	Extrusion speed /(mm/s)	Size of extrusion billets /mm	Extrusion ratio, *G*	Extrusion temperature/℃	Die shape	Lubricating mode
1#	45	Φ247	3.61	1 160-1 180	Cone die	Glass lubrication
2#	100	Φ247×Φ135×300	6.06	1 160-1 180		
3#	45	Φ247	5.04	1 160-1 180		

and they will be analyzed in the following.

2.3 Heating process before hot extrusion

Heat treatment tests were carried out on re-solution annealed material at 850-880 ℃ in a resistance furnace. Treatment time varied in the range of 1 to 4 h. The original structure was retained by water cooling after heat treatment. The samples were used for the present microstructural characterization, which was carried out using scanning electron microscopy

2.4 Microstructural analysis

The samples for test were cut from the center region of every extruded samples and ESR ingot by electronic discharging machining and then embedded in the epoxy resin for mechanical grinding and polishing. Subsequently, samples were etched with a mixture of 10 mL H_2SO_4 + 100 mL HCl + 10 g $CuSO_4$ at room temperature for 5-10 s. Microstructures of all the samples were observed on a MeF_3 optical microscope (OM; Nickon Instruments, Shanghai, China). Electron polishing and etching (90 mL methanol and 10 mL H_2SO_4) were utilized for further observation on a scanning electron microscope (SEM; FEI, Hillsboro, OR, USA), and some of the billet specimens were examined by an energy dispersive spectrometer (EDS; FEI, Hillsboro, OR, USA) on the SEM. Discs of 3 mm diameter were cut from the as-extruded samples by electronic discharging machining. Discs were ground mechanically and punched from these ground samples and were thinned by the dual jet electro polishing technique.

2.5 Electrochemical experiments

Polarization experiments were conducted in quiescent 10% NaOH and 10^{-2} Pb ions solution to distinguish the corrosion resistance as a function of processing and microstructural evolution. Pb played a crucial role in stress corrosion when materials were used as heat transfer tubeline of steam generator because it was helpful to destroy the stability of passivation membrane on alloy surface and it led to the Cr depleted near grain boundary by reducing the diffusion rate of the intracrystalline Cr to grain boundary. Electrochemical experiments were conducted using a CHI660C electrochemical workstation. Prior to each experiment, samples were polished by hand to 2000 grit using SiC paper. Scans were conducted, running from −800 mV to 800 mV using a scan rate of 10 $mV \cdot s^{-1}$. The experimental results were analyzed by Tafel extrapolation method.

2.6 Tensile test

The mechanical properties of the material before and after the extrusion were evaluated by tensile testing, which was carried out on a microcomputer controlled electronic universal testing machine (AG-10TA, Shimadzu Co. Japan) with a loading velocity of 5 $mm \cdot min^{-1}$. Samples for tensile testing with a cross-setion of 2.5 mm×2.5 mm and a gauge length of 20 mm were machined by a wire-cut machine. The test temperature was at room temperature. The tensile properties of each product, including ultimate tensile strength (UTS), yield strength (YS) and elongation to failure, were obtained based on the average value of at least three tests. Some special fracture surfaces of each group were observed on a scanning electron microscope (SEM). Thin slices were cut from tensile samples and ground to a thickness of about 150μm. Discs of 3 mm diameter were punched out and thinned using a dual-jet polishing technique in an electrolyte solution containing one part of perchloric acid and nine parts of ethanol at a temperature of about 25 ℃ and then observed in a transmission electron microscope (TEM).

3 Results

3.1 Effect on microstructure by heating process

Fig.1 shows the OM of ESR at 850 ℃ for 1h to 4h respectively. Discontinuous carbide precipitates at grain boundaries, when Inconel625 alloy is heat treated at 850 ℃. By the paper[17] we can see that the precipitates are $M_{23}C_6$ type carbide. With the prolonging of holding time, the content of carbide at grain boundary increased, and the shape of carbide was globosity when treatment time was 1 h, which changed to short rod when treatment time was 4 h.

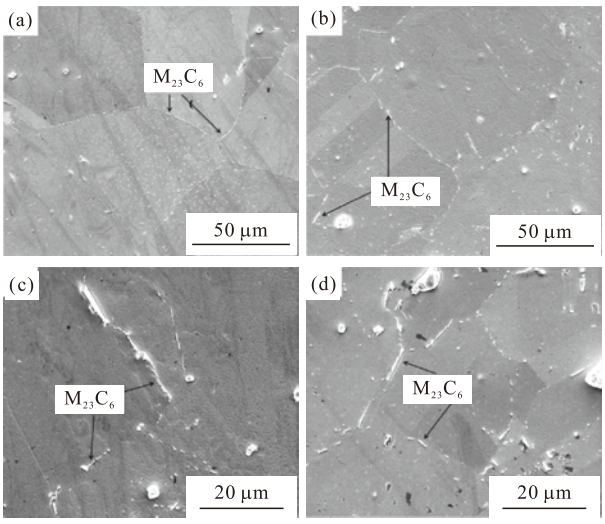

Fig.1 OM images of heat treatment microstructure of the ESR for (a) 1 h; (b) 2 h; (c) 3 h; (d) 4 h

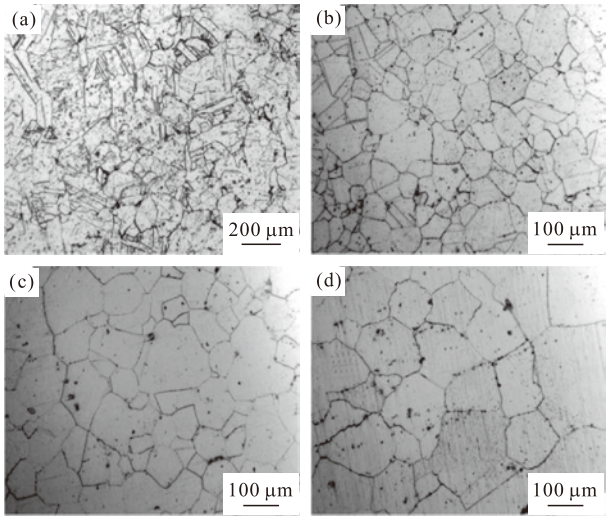

Fig.2 OM images of different states: (a) center of the ESR ingot; (b) center of bar 1#; (c) center of tube 2#; (d) center of bar 3#

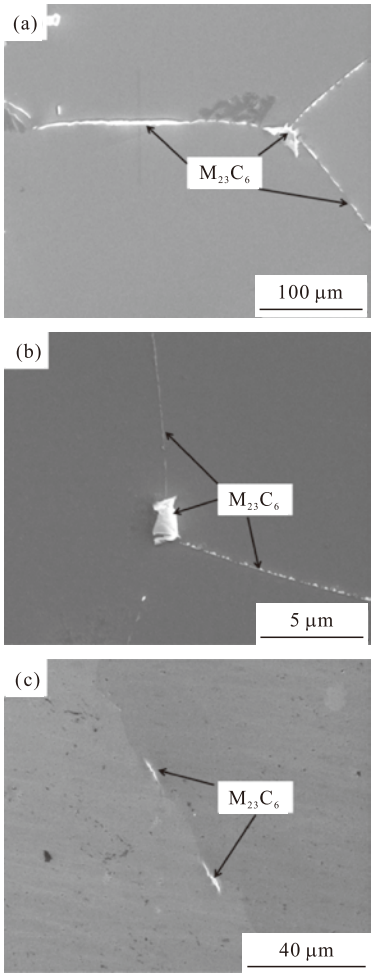

Fig.3 SEM images: (a) grain boundary morphology of sample 1#; (b) line scan of Fig.3(a); (c) grain boundary morphology of sample 2#; (d) grain boundary morphology of sample 3#

Metallographic structure of ESR ingot and extruded samples are presented in Fig.2. Fig.2(a) shows that the microstructure of the ESR ingot of Inconel 625 alloy is mainly composed of large irregular cellular crystals, characterized by a lot of deformation twins. Compared to Fig.2(a), the degree of recrystallization of hot extruded Inconel 625 alloy was excessive, and uniform equiax grains can be obtained, the size of the recrystallization grain was bigger. When the extrusion ratio was 3.61 and the extrusion speed was 45 mm/s, the grain size of sample 1# was 70 μm, as shown in Fig.2(b). At the same extrusion speed, the grain size was 135 μm when the extrusion was 5.04. The result from Fig.2(b) and Fig.2(d) indicated that the size of the recrystallization grain showed an increasing trend with increasing extrusion ratio. More deformation due to heat translated into the extrusion temperature for growing grains when the extrusion ratio was bigger. Fig.2(c) shows the microstructure of hot extruded Inconel 625 alloy with extrusion ratio of 6.06 and extrusion speed of 100 mm/s, the grain size is about 105 μm. The influence of extrusion speed, large strain rate is conducive to refine the organization for reducing the time used to grow by grains, was deemed to be the reason why the grain diminished with the aggrandizement of extrusion ratio.

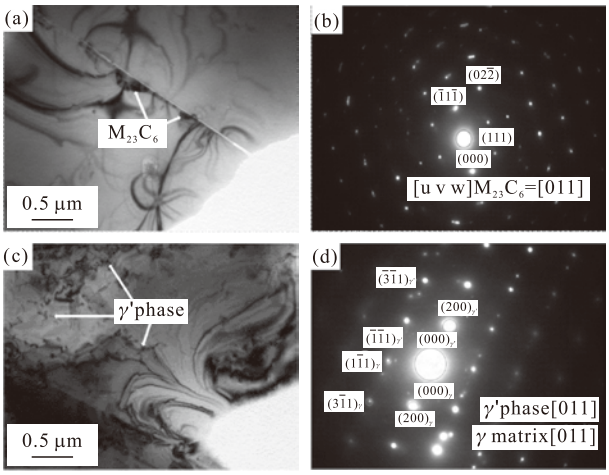

Fig.4 TEM micrographs of the Inconel 625 alloy solution after hot extrusion: (a) bright field image showing the grain boundary M23C6 carbide; (b) SAD pattern corresponding to (a); (c) bright field image showing γ phase; (d) SAD pattern corresponding to (c)

SEM microstructures of hot extruded Inconel 625 alloy specimens with different parameters are shown in Fig. 3. Fig.3(a), Fig.3(b), and Fig.3(c) are the grain boundary morphologies of samples 1#, 2#, and 3#, respectively. The $M_{23}C_6$ carbide emerged when keeping at 850-880 ℃ for a long time has a negative influence on the microstructure and properties of the material[18]. The $M_{23}C_6$ carbide exists at the grain boundary due to nucleation mechanism of alloy and grain begins to grow along a certain direction after hot extrusion[15]. A pinning effect on grain growth could be verified

for Incoenl 625 alloy in hot deformation. When the extrusion ratio was 3.61 and the extrusion speed was 45mm/s, the $M_{23}C_6$ carbide was rod-shaped and almost continuous, as shown in Fig.3(a). Most of the $M_{23}C_6$ carbide dissolves into matrix with increasing extrusion ratio during the process of hot extrusion, the $M_{23}C_6$ carbide disappeared almost, as shown in Fig.3(c). However, the content of the $M_{23}C_6$ carbide at the grain boundary in Fig.3(b) with an extrusion ratio of 6.06 and an extrusion speed of 100 mm/s was more than that in Fig.3(c). The $M_{23}C_6$ carbide had less time to dissolve with a bigger extrusion speed, and can be seen at the grain boundary as the semicontinuous graininess, despite the increase of extrusion ratio. These phases at grain boundary are deduced to be responsible for the fracture morphology of extrusions.

The microstructure of Inconel 625 alloy after extrusion presented in Fig.3 reveals the precipitation of the $M_{23}C_6$ carbide with rod-shaped morphology at the grain boundaries, however, the $M_{23}C_6$ carbide has oblate spheroidal morphology when present in the matrix. The thin foils from the hot extruded alloy were examined by TEM. The bright field image in Fig.4(a) coupled with the selected area electron diffraction pattern (SADP) in Fig.4(b) showed that the austinite matrix of the recrystallization alloy is free from others precipitates but contained intergranularly precipitated $M_{23}C_6$ carbide[19]. The other phase can be obtained by the heating and hot extrusion process, Fig.4(c) and Fig.4(d) show the typical bright field image and selected area diffraction pattern of thin film structure with (011) orientation, respectively. The secondary diffraction spots in the SADP are due to the presence of ordered $M_{23}C_6$ carbide and γ-precipitates in the matrix[20].

3.2 Electrochemical analysis

Fig.5 shows the polarization curves and electrochemical data of the Inconel 625 samples obtained in 10% NaOH and 10^{-2} Pb ion solution, and Table 3 gives the electrochemical data to indicate the corrosion resistance. E_{corr} became more negative with processing, while a decreased corrosion current density as calculated by Tafel extrapolation was found after extrusion. It can be seen that the ESR ingot has the maximum corrosion rate (1.42mpy), and this was improved by hot extrusion. The rule of corrosion rate has a similar fashion with the scale of grains after extrusion. The corrosion rate of 1# sample was the minimum, and the corrosion rate of 3# sample was the maximum. It was possible to deduce that extrusion processing of Inconel 625 led to an increase in the cathodic reaction kinetics and a concomitant decrease in the anodic reaction kinetics compared with the ESR ingot. The results of these changes in kinetics were due to a decrease in the evaluated corrosion current density (i_{corr}) and a relative reduction of the corrosion potential (E_{corr}) for extrusion processed Inconel 625 alloy.

Table 3 Electrochemical data of Inconel 625alloy

Samples	E_{corr}/mV	i_{corr}/(A/cm^2)	CPR/mpy
ESR ingot	−429.6	1.806×10^{-3}	1.420
1#	−535.2	1.315×10^{-3}	0.933
2#	−634.7	1.493×10^{-3}	1.001
3#	−741.9	1.760×10^{-3}	1.250

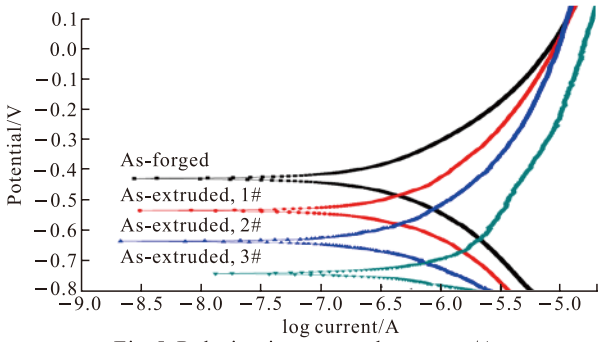

Fig.5 Polarization curves log curret/A

3.3 Tensile properties

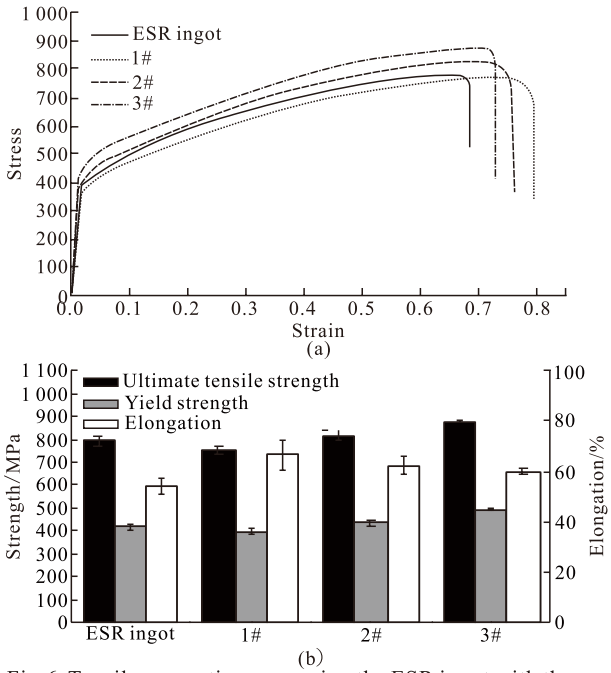

Fig.6 Tensile properties comparing the ESR ingot with the as-extruded samples: (a) stress-strain curve; and (b) histogram of the tensile properties

Fig.6 gives the tensile properties of the Inconel 625 alloy. The YS and UTS of the ESR ingot are 417 and 796 MPa, respectively, with 53.4% tensile

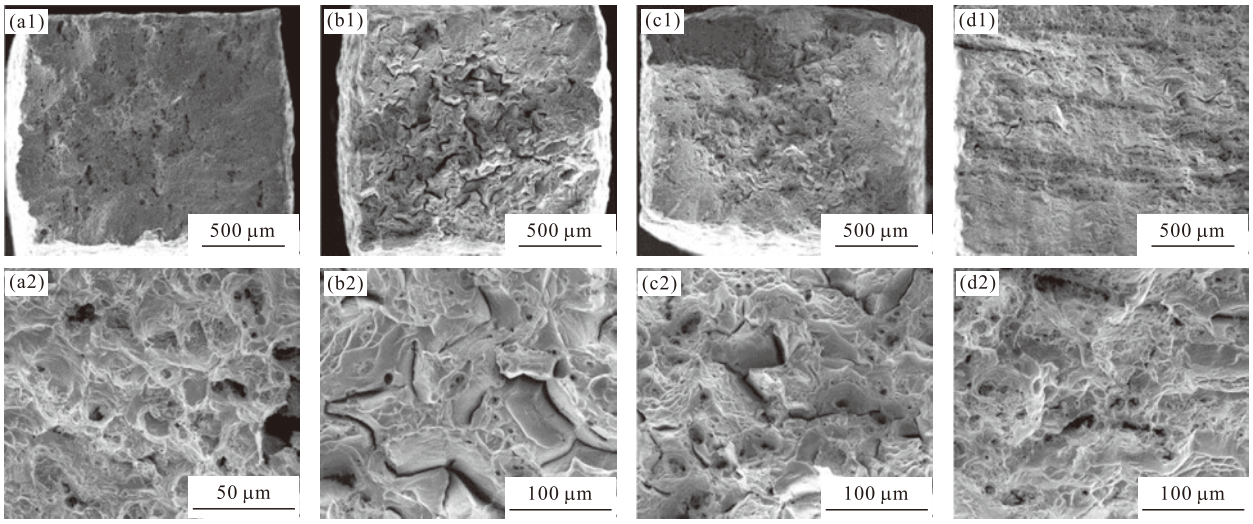

Fig.7 Fracture surface: (a1, a2) fracture of the ESR ingot; (b1, b2) fracture morphology of sample 1#; (c1, c2) fracture morphology of sample 2#; and (d1, d2) fracture morphology of sample 3#

elongation. It can be clearly seen from Fig.6 that the mechanical properties of the as-extruded sample were better than that of the ESR ingot. The UTS of specimen increased from 796 MPa to 859 MPa when the extrusion ratio was 6.06, the YS also increased from 417 MPa to 484 MPa at the same time. The extruded samples have improved ductility, as its elongation increased from 53.4% to 66.5%, when the extrusion ratio was 3.06. The difference diameter shrinkage of the as-extruded samples can be inferred from Fig.6(a), and the 3# sample has the minimum degree of the diameter shrinkage, because of a lot of cleavage planes in the fracture, as shown in Fig.7(d1).

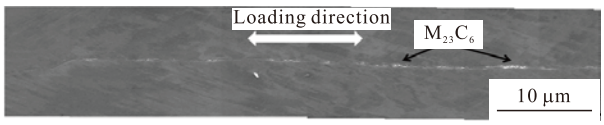

Fig.8 OM image revealing the side-view of the fracture surface of sample 1#

3.4 Tensile fracture surface

The evolution of the tensile fracture surface as a function of processing is presented in the SEM fractographs in Fig.7. Typical microstructural characteristics of ductile fracture, dimples and tearing ridge can be seen in the tensile fracture surface morphology of the ESR ingot, as presented in Fig.7(a). It can be seen that the fracture surface had an obvious change after extrusion. There were many cleavage planes, secondary cracks, tearing ridges, and dimples in Fig.7(b), typical of a quasi-cleavage fracture morphology. With the increase of the extrusion ratio, the number of secondary cracks remarkably reduced, and the surface of the secondary crack became thin and long. However, the more cleavage planes indicate the enhancement of cleavage fracture, as shown in Fig.7(d). Fig.7(c) shows the fractograph of the hot extruded tube with an extrusion ratio of 6.06 and an extrusion speed of 100 mm/s. The fracture characteristics make ductility and toughness are higher than that of the ESR ingot: the tearing ridge, dimples and a large number of secondary cracks are clearly observed. On the basis of Fig.3 and Fig.7, Fig.8 shows the side-view of the fracture surface of the sample after hot extrusion. The intergranular crack can be seen, and the crack was more obvious with the distribution of the $M_{23}C_6$ carbide at the grain boundary. All of these proved that the $M_{23}C_6$ carbide has an important impact on properties.

4 Discussion

4.1 Improved corrosion resistance

The grain size alone has been shown for other alloys to have a marked impact on the corrosion rate, depending on the environment and the alloy. The relative dissolution or passivation of a surface has been linked to the total grain boundary length, which is considered as a proxy for the overall surface reactivity and diffusivity and plays a critical role in the corrosion and passivation processes. Depending on specific material/ environment combinations, an increased grain boundary density can either increase or decrease the corrosion. The main corrosion mechanism of superalloys has been proven to be intergranular corrosion occurring in an acid and hot corrosive environment[21-23]. The $M_{23}C_6$ carbide contains plenty of Cr element at the grain boundary and has a more important effect on the corrosion rate by forming Cr_2O_3 oxide film. A relative decrease is observed in

the contents of Nb and Cr, which can be considered as dissolution of these elements into the environment induced by the presence of the characteristic features on the exposition surface. Nb forms a protective surface film when placed in acidic or alkaline solution, and a decrease in the chemical dissolution rate of oxide films has been shown with the increase of the Nb content in a NaOH solution[24].

4.3 Tensile fracture surface and strengthening mechanisms

To verify the fracture mechanism of the ESR ingot and extrusions of Inconel 625 alloy, the microstructure obtained after extrusion is discussed in light of the TEM images. After elastic deformation, plastic deformation occurs with the change of the microstructure in the tensiling process. Plenty of dislocations appear; slip with the deformation and piling up of dislocations will emerge near the grain boundary and areas of element segregation, as shown in Fig.9(a). Subsequently, dislocations across the grain boundary will cut the particles consisting of segregated elements, for example, Nb, Mo, and Ti, and secondary phase when the degree of dislocations pile-up is strong enough. The original cracks formed from the fracturing of the particles by slipping of the dislocations are elongated to become cavities along the direction of tensile elongation. Fractures will take place when the cavities connect to each other as the tensile process further progresses. Thus, the particles cut by dislocations are located in the center of the dimples on the fracture morphology of the ESR ingot.

Grains deform in the drawing process and elongate along the tensile direction during tensile testing. However, the $M_{23}C_6$ carbide at the grain boundary, which does not have a good ductility, would be crushed by the slipping of adjacent grains, leading to the separation of adjoining elongated grains, as shown in Fig.8. As the tension continues, the shrinkage diameter of the tensile samples can be decomposed into the shrinkage diameter of each grain. Because the contents of the $M_{23}C_6$ carbides at grain boundary are not continuous, a small amount of grains can fail by intergranular fracture, while others fail via ductile fracture, such as in the ESR ingot. Gaps between the grains are obtained when grains break, which are called secondary cracks. However, the number of secondary cracks decreases with the increase of the extrusion ratio and increases with the decrease of the extrusion speed, which shows that the temperature plays a decisive role in forming secondary cracks. In other words, the content of the $M_{23}C_6$ carbide is determined by the extrusion temperature, which affects the fracture morphology[25]. On the other hand, due to the low stacking fault energy of the Inconel 625 alloy at room temperature, the alloy could also proceed with a twin coordination deformation, where the grain orientation can change to generate the location of the twin when dislocation glides are hindered during the tensile process[26]. The twin deformation can reduce the concentration of stress in the deformed part, enhance the tenacity of the alloy, and change the direction of crack propagation, as shown in Fig.7(b2). Deformation twins from twin coordination deformation can hinder the subsequent dislocation glide, and stress concentration will arise at the twin boundary where dislocations are more and more heavily concentrated (Fig.9(b)). Along with the deformation, concentration of dislocation will cross the twin boundary and slip again when the stress concentration is large enough. The stress concentration at the twin boundary increases and a large concentration of dislocation can pass through the twin boundary when the crack extends to the twin boundary. With the above knowledge, there is difference in the crystal orientation on both sides of the twin boundary, which leads to crack deflection when the crack crosses the twin boundary. All of these create ups and downs of the fracture morphology significantly. From what has been discussed above, the fracture surface and deformation mechanism consist of dislocation slip and twin coordinate deformation.

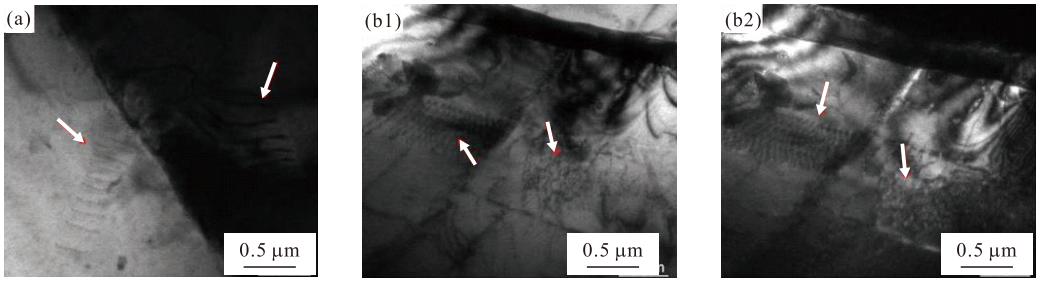

Fig.9 TEM images: (a) dislocation pileup near the grain boundary; and (b1, b2) the bright field image and dark field of the dislocation pileup near the twin boundary

It is well known that Nb has a large atomic radius which gives rise to difficult diffusion and easy segregation. It can be seen that plenty of segregated Nb (black spots) is located in the matrix in Fig.2. As a solid solution strengthening alloy, Nb dissolved in the Inconel 625 has an important influence on the tensile properties[27]. The segregation can be seen in the heart of the dimples in both ESR ingot and extruded samples in Fig.10, but the content of Nb in the segregated zone is different, *i e*, 88.7%, 77.1%, 71.7%, and 55% (quality percentage) for ESR ingot, samples with extrusion ratios of 3.61, 6.06, and 5.04, respectively. This perfectly explains the changing strength of the extrusions, the recrystallized structure from hot extrusion takes away the residual stress due to the ESR ingot, which explains why the strength of the material with a small amount of Nb dissolved into the matrix with an extrusion ratio of 3.61 did not increase. As stated above, the actual extrusion temperature will be improved with the increase of the extrusion ratio when the extrusion speed is constant; the sample with an extrusion ratio of 5.04 has the highest strength. This indicates that high temperature is beneficial for diffusion. It can be inferred that the diffusion of Nb was hindered from Fig.10(c) and Fig.10(d). Although when the extrusion ratio was 6.06, the strength was not the highest[24,28]. The extrusion time should be considered at a high temperature because the extrusion process is completed before a large degree of diffusion occurs. In addition, the austenitic nickel-based alloy deforms plastically during tensile testing, while the segregation Nb and carbide are rigid and deform only elastically. Therefore, a high stress concentration generates at the interface of the particles/matrix. The fragmentation of the compound particles generated by the stress concentration is an indication of the absorption of energy and relaxation of local stress concentration. This delays the growth rate and nucleation of the cracks in the surrounding matrix[29]. To sum up, the mechanism of the solution strengthening of the Nb element is the additive or synergetic effect by combining with a load transfer mechanism.

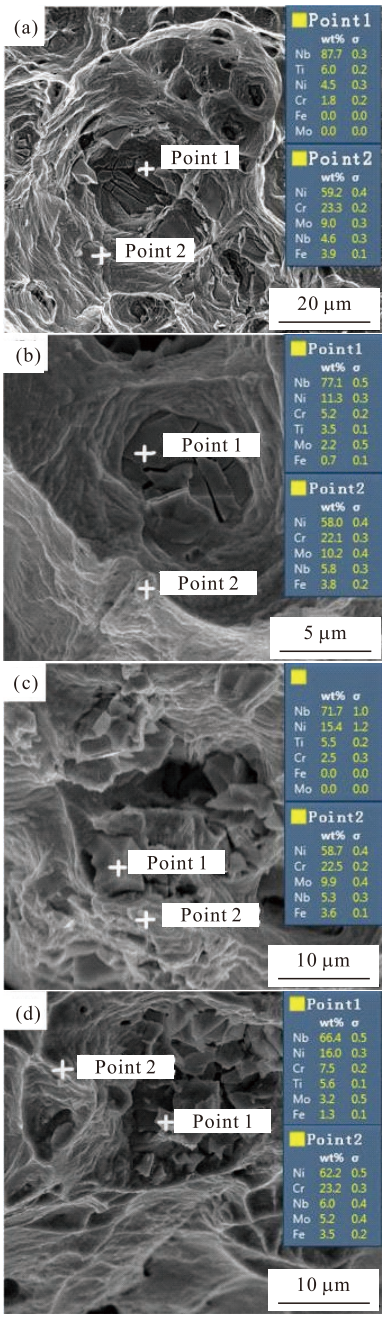

Fig.10 SEM images and EDS data: (a) EDS data of the ESR ingot; (b) EDS data of sample 1#; (c) EDS data of sample 2#; (d) EDS data of sample 3#

5 Conclusions

a)By comparing the microstructure, fracture morphology, and corrosion resistance from the forging and extrusions, the $M_{23}C_6$ carbide was generated in the process of heat treatment and remained at the grain boundary after extrusion, converting the fracture mechanism from a ductile fracture to a quasi-cleavage fracture. The process of heating was significant prior to extrusion.

b)The average grain size increased with the increase of extrusion ratio. Better microstructure would be achieved when the extrusion speed was controlled between 100 mm/s-160 mm/s.

c)With the increase of the real extrusion temperature, the $M_{23}C_6$ carbide and segregation Nb dissolved into the matrix to make a stronger solid solution strengthening and improving the strength, as

well as boosting the corrosion rate due to the special technique. However, the $M_{23}C_6$ carbide and segregation Nb did not have enough time to diffuse when the extrusion time was short at a high extrusion speed, and the opposite result was obtained.

d)The strengthening mechanism of the solution strengthening of Nb element is the additive or synergetic effect in combination with the load transfer mechanism.

References

[1] Holcomb GR. High Pressure Steam Oxidation of Alloys for Advanced Ultra-supercritical Conditions[J]. *Oxid Met*., 2014, 82: 271-295

[2] Oksa M, Metsajoki J, Karki J. Thermal Spray Coatings for High-temperature Corrosion Protection in Biomass Co-fired Boilers[J]. *J Therm. Spray Techn.*, 2015, 24: 194-205

[3] Oksa M, Tuurna S, Varis T. Increased Lifetime for Biomass and Waste to Energy Power Plant Boilers with Hvof Coatings: High Temperature Corrosion Testing under Chlorine-containing Molten Salt[J]. *J. Therm. Spray Techn.*, 2013, 22: 783-796

[4] Liu DX, Guo CG, Chai LQ, *et al.* Meyers, M.A. Mechanical Properties and Corrosion Resistance of Hot Extruded Mg-2.5Zn-1Ca Alloy[J]. *Materials Science and Engineering: B*, 2015, 195: 50-58

[5] Yu ZJ, Huang YD, Mendis CL, *et al*. Microstructural Evolution and Mechanical Properties of Mg-11Gd-4.5Y-1Nd-1.5Zn-0.5Zr Alloy Prepared Via Pre-ageing and Hot Extrusion[J]. *Materials Science and Engineering: A*, 2015, 624: 23-31

[6] Loginov YN, Demakov SL, Illarionov AG, *et al*. Evolution of Defects in the Production of Capillary Copper Tubes[J]. *Journal of Materials Processing Technology*, 2015, 224: 80-88

[7] Guo SL, Li DF, Guo QM, *et al*. Investigation on Hot Workability Characteristics of Inconel 625 Superalloy Using Processing Maps[J]. *Journal of Materials Science*, 2012, 47: 5 867-5 878

[8] Dong JX, Zhang MC, Zeng YP, *et al*. Phase Transformation and Characteristics in Freckle Areas for Inconel625 Superalloy[J]. *A Xie cta Metallurgica Sinica*, 2005, 18: 47-54

[9] Wang L, Wang S, Song X, *et al*. Effects of Precipitated Phases on the Crack Propagation Behaviour of a Ni-based Superalloy[J]. *International Journal of Fatigu*, 2014, 62: 210-216

[10] Cheng M, Zhang HY, Zhang SH. Microstructure Evolution of Delta-processed in718 During Holding Period After Hot Deformation[J]. *Journal Of Materials Science*, 2012, 47: 251-256

[11] Chen F, Liu J, Ou HG, *et al*. Flow Characteristics and Intrinsic Workability of IN718 Superalloy[J]. *Mat. Sci. Eng. A-Struct*., 2015, 642: 279-287

[12] Sun C Y, Liu J R, Li R, *et al*. Constitutive Relationship of IN690 Superalloy by Using Uniaxial Compression Tests[J]. *Rare Metals*, 2011, 30: 81-86

[13] Guo QM, Li DF, Guo SL, *et al*. The Effect of Deformation Temperature on the Microstructure Evolution of Inconel 625 Superalloy[J]. *Journal of Nuclear Materials*, 2011, 414: 440-450

[14] Wang SY, Dong YP, Zhang MC, *et al.* Study on the Recrystallization Behavior of an As-extruded pm Superalloy[J]. *Applied Mechanics and Materials*, 2014, 529: 71-78

[15] Guo QM, Li DF, Peng HJ, *et al*. Nucleation Mechanisms of Dynamic Recrystallization in Inconel 625 Superalloy Deformed with Different Strain Rates[J]. *Rare Metals*, 2012, 31: 215-220

[16] Li DF, Wu ZG, Guo SL, *et al*. Study on the Processing map of GH625 Ni-based Alloy Deformed at High Temperature[J]. *Rare Metal Materials and Engineering*, 2012, 41: 1 026-1 031(in Chinese)

[17] Ferrer L, Pieraggi B, Uginet JF. Microstructual Evolution during Thermomechanical Proeessing of Alloy625[J]. *The Materials, Metals & Materials Soeiety*, 1991: 217-228

[18] Shankar V, Rao KBS, Mannan SL. Microstructure and Mechanical Properties of Inconel625 Superalloy[J]. *Jo urnal of Nuclear Materials*, 2000, 288: 222-232

[19] Raoa GA, Srinivasa M, Sarmab DS. Effect of Solution Treatment Temperature on Microstructure and Mechanical Properties of Hot Isostatically Pressed Superalloy Inconel 718[J]. *Mater. Sci. Tech-Lond*., 2004: 1 161-1 170

[20] Yun SL, Dong JK, Seong SH, *et al*. $M_{23}C_6$ Precipitation Behavior and Grain Boundary Serration in Ni-based Alloy 690[J]. *Materials Characterization*, 2014, 96: 28-39

[21] Weng F, Yu H, Chen CZ, *et al*. Influence of Nb and Y on Hot Corrosion Behavior of Ni-Cr-based Superalloys[J]. *Materials and Manufacturing Processes*, 2014, 30: 677-684

[22] Buscacil H, Rolland R, Issartel C, *et al.* Effects of Water Vapour on the Oxxidation of a Nickel- base 625alloy between 900 and 1 100 ℃[J]. *J. Mater. Sci.*, 2011, 4: 5 903-5 915

[23] E Mohmmadi Zahrani, AM Alfantazi. Corrosion Behavior of Alloy 625 in PbSO-PbO-PbCl-ZnO-10Wt Pct CdO Molten Salt Medium[J]. *Metallurgical and Materials Transactions A*, 2012, 43A: 2 857-2 868

[24] Rosalbino F, Macciò D, Saccone A, *et al*. Effect of Nb Alloying Additions on the Characteristics of Anodic Oxide Films on Zirconium and Their Stability in Naoh Solution[J]. *Journal of Solid State Electrochemistry*, 2009, 14: 1 451-1 455

[25] Tae HL, Young JL, Sin Hyeon, *et al.* Intergranular $M_{23}C_6$ Carbide Precipitation Behavior and Its Effect on Mechanical Properties of Inconel690 Tubes[J]. *The Materials, Metals & Materials Soeiety*, 2015, 46A: 4 020-4 026

[26] Wang ZT, Zhang XY, Deng Y G, *et al.* Twins and Texture of Super-alloy IN690 Tube by Extrusion[J]. *Rare Metal Materials and Engineering*, 2014, 43: 2 252-2 256

[27] Du JH, Lu XD, Tang C, *et al*. Effects of P and Nb on Mechanical Properties of GH4169 Alloy[J]. *Mater. Res. Innov*., 2014, 18: S4-375-S374-379

[28] Gulsoy HO, Pazarlioglu S, Gulsoy N, *et al*. Effect of Zr, Nb and Ti Addition on Injection Molded 316L Stainless Steel for Bio-applications: Mechanical, Electrochemical and Biocompatibility Properties[J]. *Journal of the Mechanical Behavior of Biomedical Materials*, 2015, 51: 215-224

[29] Zhang SQ, Chen TJ, Cheng FL, *et al*. A Comparative Characterization of the Microstructures and Tensile Properties of as-cast and Thixoforged in Situ AM60B-10vol% Mg2Sip Composite and Thixoforged AM60B[J]. *Metals*, 2015, 5: 457-470